



FUJI Dome: A large detachment fault near 64°E on the very slow-spreading southwest Indian Ridge

R. C. Searle

Department of Geological Sciences, University of Durham, DH1 3LE, UK (r.c.searle@durham.ac.uk)

M. Cannat

CNRS, Laboratoire de Géosciences Marines, Institut de Physique du Globe, 4 place Jussieu, 75252 Paris cédex, France (cannat@ccr.jussieu.fr)

K. Fujioka

Japan Marine Science and Technology Center, 2-15 Natsushima-cho, Yokosuka, 237-0061 Japan (fujiokak@jamstec.go.jp)

C. Mével

CNRS, Laboratoire de Géosciences Marines, Institut de Physique du Globe, 4 place Jussieu, 75252 Paris cédex, France (mevel@ccr.jussieu.fr)

H. Fujimoto

Research Center for Prediction of Earthquakes and Volcanic Eruptions, Faculty of Science, Tohoku University, Aoba-ku, Sendai 980-8578, Japan (fujimoto@aob.geophys.tohoku.ac.jp)

A. Bralec

Department of Geological Sciences, University of Durham, DH1 3LE, UK

Now at Shell International Exploration and Production, Volmerlaan 8, Postbus 60, 2280 AB Rijswijk, Netherlands (Abigail.Bralec@shell.com)

L. Parson

Southampton Oceanography Centre, Empress Dock, Southampton SO14 3ZH, UK (lmp@soc.soton.ac.uk)

[1] A continuous, domed detachment surface (FUJI Dome) has been imaged on the very slow-spreading southwest Indian Ridge using deep-towed side-scan sonar, and has been investigated by manned submersible and sea-surface geophysics. The Dome is morphologically similar to other oceanic detachments, core complexes or mega-mullions. In addition to bathymetric mullions observed in ship-borne bathymetry, finer scale spreading-parallel striations were imaged with the side scan. On the detachment surface, metabasalt crops out near the termination, probably as part of a thin fault sliver. Gabbro and troctolite probably crop out near the summit of the dome. The rest of the detachment surface is covered with sediment and rubble which is basaltic except for a single sample of serpentinite. Most of the detachment surface dips toward the ridge axis at 10°–20°, but near the breakaway it is strongly rotated outward, and dips away from the axis at up to 40°. Normal, undeformed volcanic seafloor crops out adjacent to the detachment. Modeling of sea surface magnetic data suggest the detachment was active from 1.95 Ma for about 1 Ma during a period of reduced and asymmetric magmatic accretion. Modeling of sea surface and seafloor gravity requires laterally fairly uniform but high density material under the Dome, and precludes steeply dipping contacts between bodies with large density contrasts at shallow levels under the Dome.

Components: 11,430 words, 7 figures, 2 tables.

Keywords: Southwest Indian Ridge; detachment; submersible; magnetic; gravity.

Index Terms: 3035 Marine Geology and Geophysics: Midocean ridge processes; 3045 Marine Geology and Geophysics: Seafloor morphology and bottom photography.

Received 7 February 2003; **Revised** 17 June 2003; **Accepted** 19 June 2003; **Published** 8 August 2003.

Searle, R. C., M. Cannat, K. Fujioka, C. Mével, H. Fujimoto, A. Bralee, and L. Parson, FUJI Dome: A large detachment fault near 64°E on the very slow-spreading southwest Indian Ridge, *Geochem. Geophys. Geosyst.*, 4(8), 9105, doi:10.1029/2003GC000519, 2003.

Theme: Accretionary Processes Along the Ultra-Slow Spreading Southwest Indian Ridge
Guest Editors: Catherine Mevel and Daniel Sauter

1. Background

[2] For some time it has been hypothesized that an important mode of seafloor spreading at slow-spreading ridges is asymmetric extension along long lasting, possibly low-angle, normal “detachment” faults [Karson, 1990; Lagabriele *et al.*, 1998]. Such faults may expose the lower crust or even upper mantle [Tucholke *et al.*, 1997]. One school of thought is that they alternate with episodes of roughly symmetric, predominantly “magmatic” extension [Tucholke *et al.*, 1997; Varga and Moores, 1990], on a timescale of several million years, but a contrasting view is that such faulting may be a more-or-less continuous aspect of plate separation in regions of permanently low magma supply [Cannat and Casey, 1995; Lagabriele *et al.*, 1998].

[3] Approximately 22 such features have been recognized to date on the Mid-Atlantic Ridge (MAR) [Cann *et al.*, 1997; Fujiwara *et al.*, 2003; Reston *et al.*, 2002; Tucholke *et al.*, 1998a]. Their recognition was based on sea-surface multibeam bathymetry data, which usually show a characteristic doming of the seafloor together with small-scale topographic corrugations lineated parallel to the spreading direction (“mullions”), and often narrow valleys at the “breakaway” (the point on the footwall where the fault began) and the “termination” (the point on the hanging wall where it ended). Cann *et al.* [1997] imaged two such features at the Atlantis Transform on the MAR,

using Southampton Oceanography Centre’s TOBI deep-towed side-scan sonar. They imaged striations parallel to the spreading direction and suggested that these represent alternating outcrops and sediment-filled grooves. Those corrugated domes that have been sampled are mostly associated with gabbros or serpentinised peridotites and basalts. These observations suggested that the features may be “oceanic core complexes” analogous to the metamorphic core complexes exposed by low angle normal faulting in the western USA [Davis, 1987; Lister and Davis, 1989]. Domed corrugated surfaces near present-day ridges have thus been interpreted as the fossil footwalls of former detachment faults and have been termed “megamullions” [Tucholke, 1997]. If such detachments expose lower crust or upper mantle, they provide an important opportunity to directly study the lithology and structure of this part of the young oceanic lithosphere, together with the tectonic and magmatic processes that were associated with its formation and evolution.

[4] A few oceanic megamullions have now been investigated by submersible [Karson, 1998; Matsumoto *et al.*, 1998; Tucholke *et al.*, 2001] and one has been extensively sampled using a wire line rock drill [MacLeod *et al.*, 2002]. This last study successfully demonstrated for the first time that the dome’s corrugated surface was indeed a former detachment fault surface: drilled samples are fault rocks with low-angle shear planes and highly deformed greenschist facies assemblages.

[5] Known examples of oceanic megamullions are all low-angle and some even dip away from the spreading axis. However, the attitude of the detachment faults at depth and while active is unknown: competing hypotheses predict either a continuing shallow dip below the surface [Karson, 1990; Varga and Moores, 1990], or a steeply dipping fault plane that subsequently rotates over a hinge [Lavier et al., 1999; Shemenda and Grocholsky, 1994; Tucholke and Lin, 1994]. In the latter case, significant (approaching 90°) rotation must occur during fault movement. Buck [1988] presented a model in which large rotations can be achieved by repeated small tilts on a succession of high-angle faults, which may fit continental [Lister and Davis, 1989], ophiolite [Varga and Moores, 1990] and some mid-ocean ridge cases [Karson, 1990] where there is evidence of multiple high-angle and low-angle faulting. Buck's model also predicts a high flexural rotation and steep dip on the hanging wall of the detachment. Subsequently, Lavier et al. [1999] have produced numerical models of extension in oceanic lithosphere, showing that under conditions that promote strain localization and softening, detachment faults can form, rotating the footwall through large angles so that the upper part of the fault plane can dip away from the spreading centre. Determining the geometry and rotation of the fault plane during the formation of mega-mullions is vital for a detailed understanding of how oceanic lithosphere extends.

[6] Another aspect of megamullion formation that needs further study is that, although slow spread oceanic lithosphere shows widespread evidence for extensive normal faulting and the exposure of deeply derived rocks (gabbros and peridotites), megamullions are rather infrequently observed [Tucholke et al., 1998a]. Tucholke et al. [2003] propose that very long-lasting and large offset faults that lead to the formation of megamullions only form under conditions where there is a delicate balance between magma supply and tectonic extension.

[7] In October 1997 we carried out a TOBI survey on the very slow spreading (half rate 7 km Ma⁻¹) southwest Indian Ridge during the FUJI (France-UK-Japan-InterRidge) cruise [Mével et al., 1997a; Mével et al., 1998], during the

course of which we serendipitously imaged a previously unknown detachment in its entirety (Figures 1 and 2). We have named this feature the FUJI Dome. It was subsequently the target of three dives with the manned submersible Shinkai 6500 during the *Indoyo* cruise in September–October 1998 (Figure 3) [Fujimoto et al., 1998; Fujimoto et al., 1999]. Here we report our findings.

2. Data

[8] The 1997 FUJI cruise was dedicated to a TOBI survey. The TOBI deep-towed instrument [Flewelling et al., 1993] carried 30 kHz side-scan sonar with nominal horizontal resolution of 6 m and swath width of 6 km, phase bathymetry with similar resolution horizontally and vertically, and three-component magnetometer. The tow-ship, *Marion Dufresne*, deployed a Thomson multi-beam echo sounder and proton magnetometer. The TOBI side scan worked well, but its swath bathymetry phase data were very noisy and have proved of limited value. The TOBI magnetometer broke down earlier in the cruise, and despite an attempted on-board repair, we have not been able to recover trustworthy data from it. This was the first cruise on the *Marion Dufresne* of the Thomson echo sounder, which had significant teething problems and also produced relatively noisy data. Finally, the *Marion Dufresne*'s magnetometer was out of action for much of the FUJI Dome survey.

[9] The *Indoyo* cruise of *R/V Yokosuka* deployed a SeaBeam 2000 multibeam, together with gravimeter and proton magnetometer, all of which were used to survey off-axis during nighttime, and produced good data. Gravity data were tied to a base station in Port Louis, Mauritius, and magnetic data were reduced to the IGRF. We have supplemented the multibeam bathymetry with earlier data obtained over the ridge axis by the French CAPSING and GALLIENI cruises [Patriat et al., 1996].

[10] The main objective of the *Indoyo* cruise was a diving program with the manned submersible *Shinkai 6500*. Three of the dives (numbers 444, 445 and 450) were dedicated to the FUJI Dome (Figure 3). All of them carried out visual observations, made continuous video and still camera

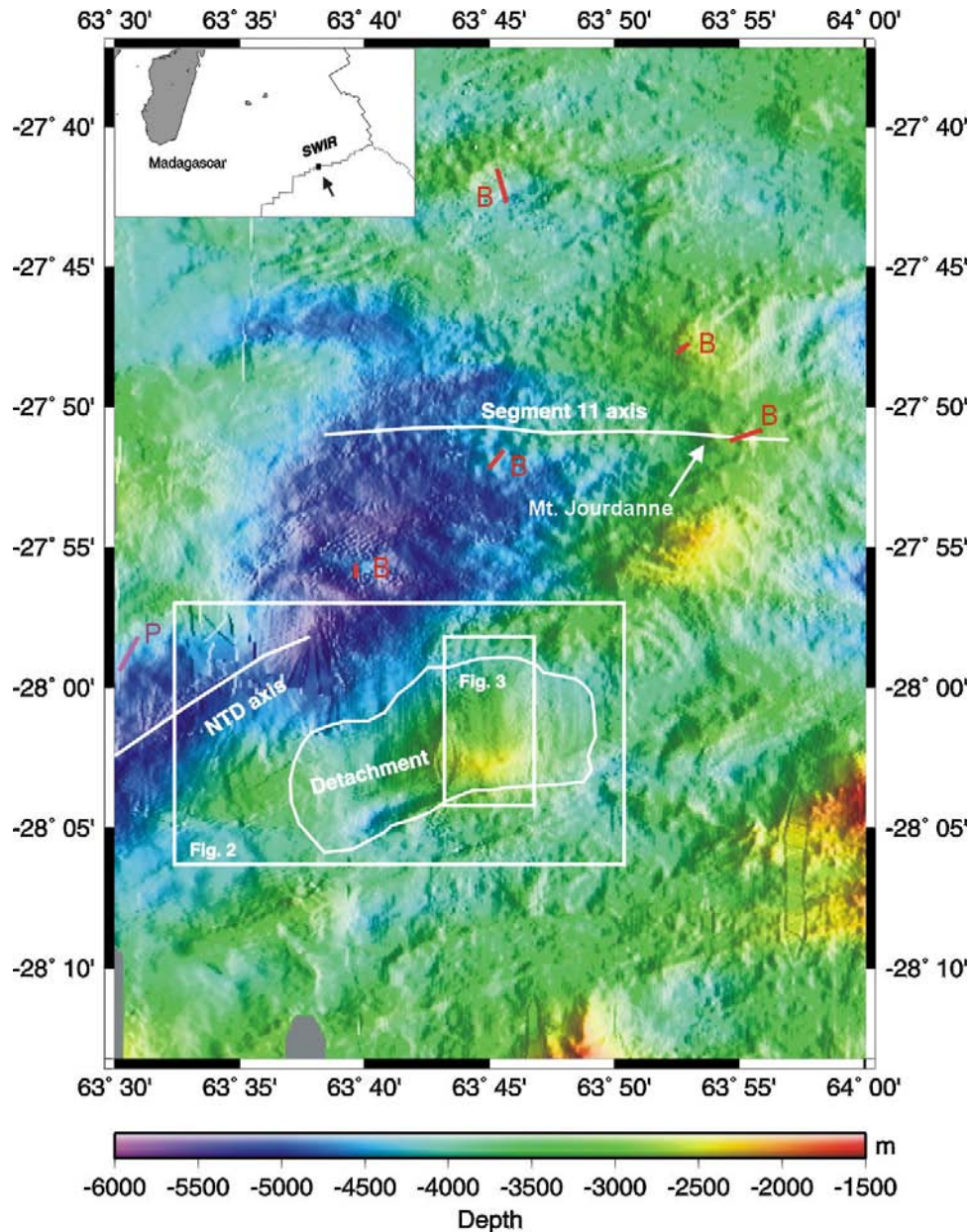


Figure 1. Seafloor topography (shaded relief, illuminated from east, depth in meters), showing the FUJI Dome on the southern flank of the southwest Indian Ridge. Red bars marked “B” show positions of basalt dredges; purple bar marked “P” a peridotite dredge [Mével *et al.*, 1997a]. Inset shows regional location, with study area arrowed.

recordings, and collected rock and sediment samples (Table 1). Gravity was measured within the submersible at one station on each dive, using a Lacoste & Romberg Geodetic meter G-1039 tied to a base station in Port Louis (Table 2).

3. Regional Setting

[11] The spreading segment within which the FUJI Dome lies was covered by a detailed TOBI survey

which will be reported elsewhere [Bralee, 2003 and A. V. Bralee, MS in preparation]. Interpretation of this survey revealed a typical volcanic terrain flanking a well-developed axial volcanic ridge (AVR) which culminates in the large volcanic massif of Mont Jourdanne at 27°52'S, 63°55'E (Figure 1) [Bralee, 2003; Mével *et al.*, 1998; Searle *et al.*, 1998b]. This volcanic terrain tapers to the west, suggesting that the tip of the AVR (though not necessarily the tectonic boundary of the seg-

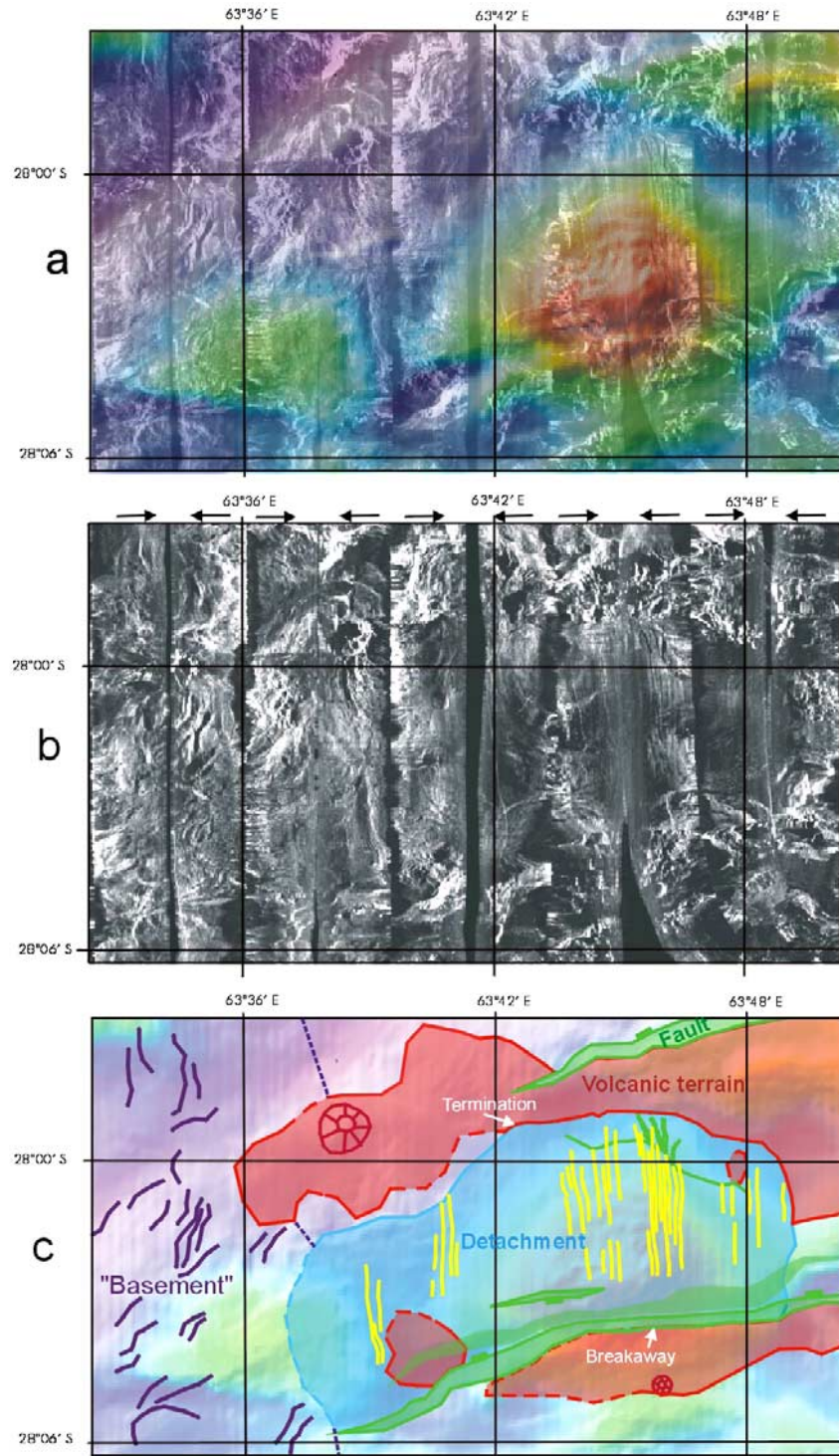


Figure 2. (a) TOBI side scan mosaic overlain by coloured bathymetry in the area of the FUJI Dome detachment. (b) Side-scan sonar mosaic, corrected for slant-range distortion and variations in vehicle height. Light tones represent strong acoustic backscatter. Arrows at top of image show insonification direction for each swathe. (c) Geological interpretation based on side scan and bathymetry superimposed on bathymetry image. Red, volcanic terrains and volcanoes; blue: detachment surface; yellow, spreading-parallel lineaments on detachment; green, normal faults; purple, curved lineaments of "basement" terrain (see text). Outlines are dashed where uncertain. See Figure 1 for location.

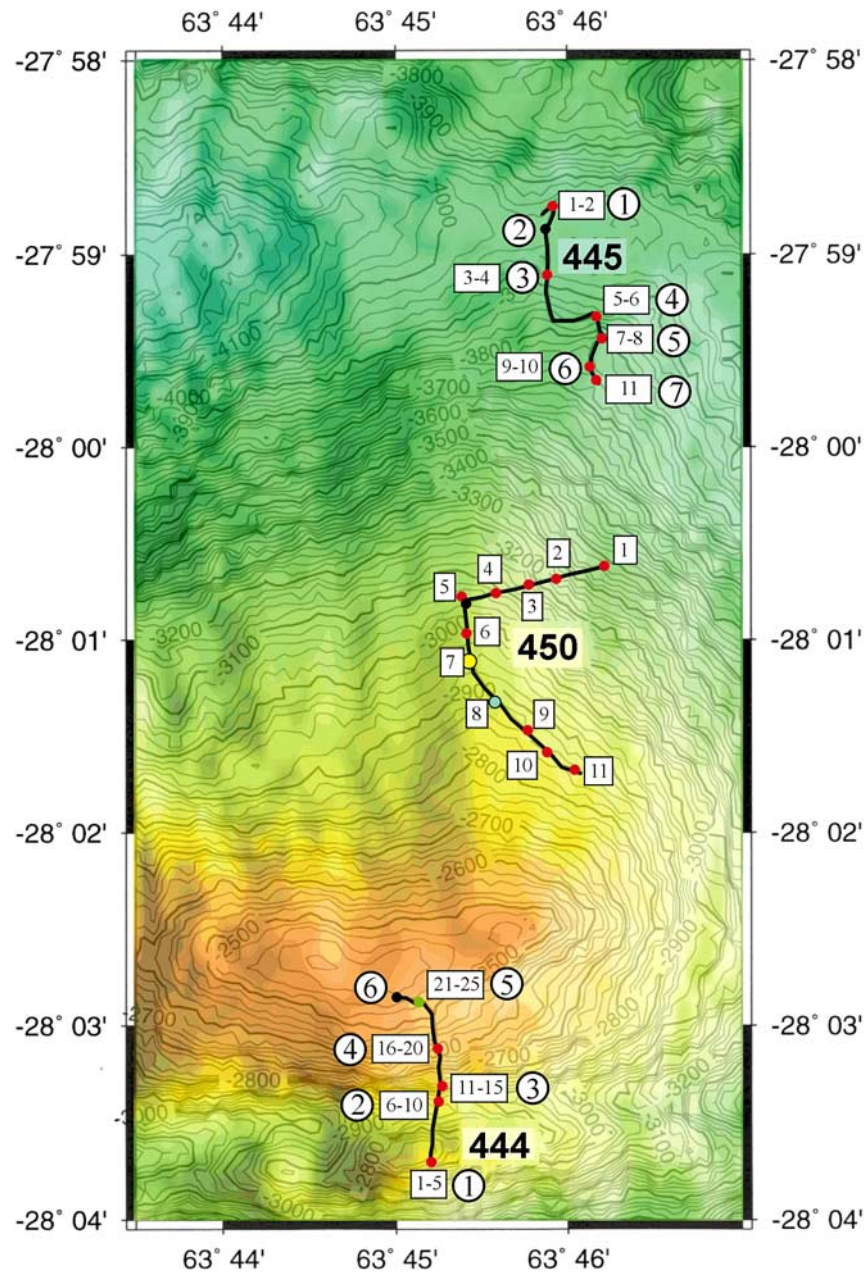


Figure 3. (a) Detailed bathymetry over the area of the *Shinkai* dives. Contour interval 20 m. Dive tracks and rock sampling stations are superimposed. Boxes give sample numbers (see Table 1), and are coloured according to lithology: red, basalt; green, gabbro; blue, serpentinite; yellow, sediment. Black dots show positions of gravity stations. Circled numbers indicate station numbers (see Figure 7). For Dive 450, there was one sample from each station so station number is the same as sample number. (b) Detail of the TOBI side-scan sonar image over the same area, with dive tracks and stations, coloured as in left panel, superimposed. Light tones of side scan are high backscatter. White arrows at left and right edge of image show insonification directions. (c) Side scan image with interpretation, using same colour code as Figure 2, superimposed.

ment) has propagated westward over the past few million years. It now abuts a large escarpment that forms the NW flank of the adjacent non-transform discontinuity (NTD) near 63°38'E (Figure 1). FUJI

Dome lies some 20 km south of the AVR and east of the NE-SW trending NTD, and is thus in an inside corner position. Six dredges have been reported from the area, though none was from the

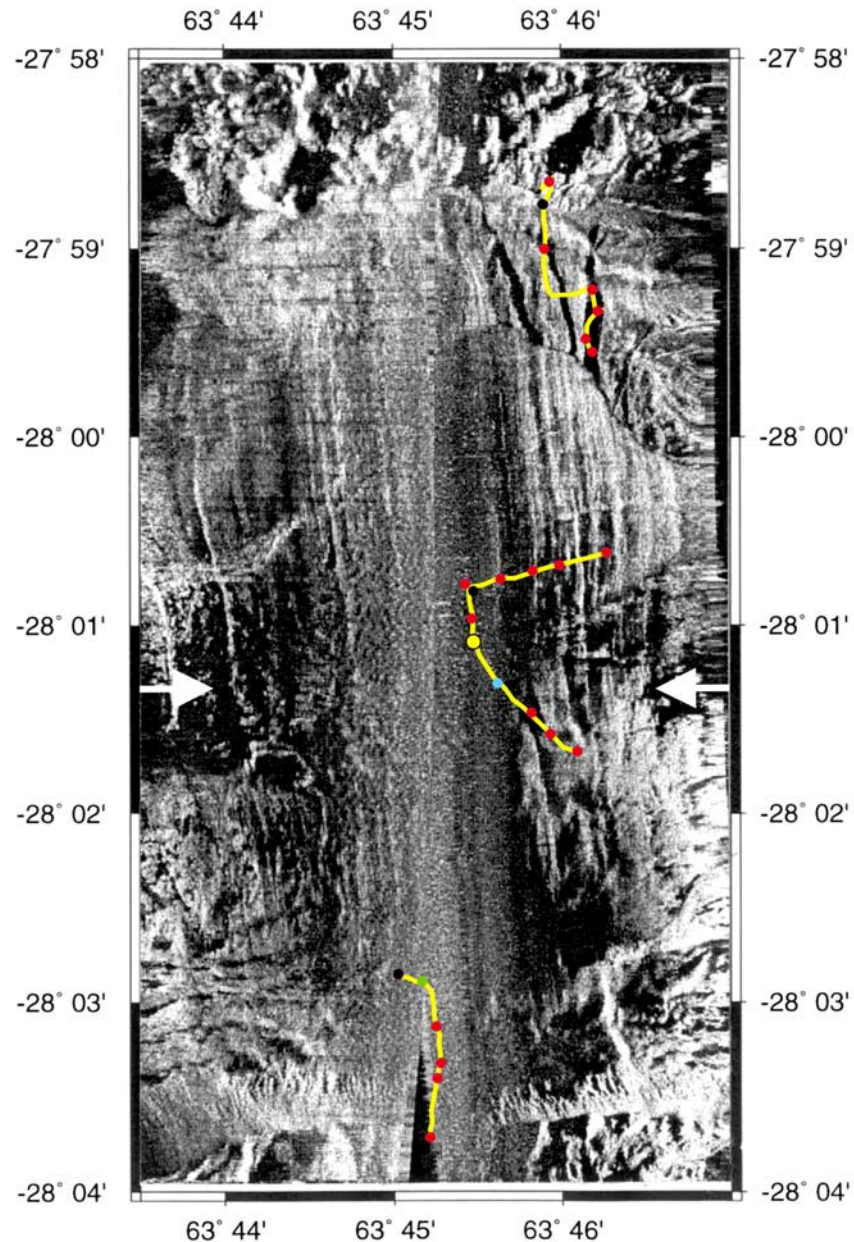


Figure 3. (continued)

detachment [Mével *et al.*, 1997a]. Five, from the ridge axis and flanks, contained basalt, and the sixth, from the NW flank of the NTD, recovered serpentinized peridotite (Figure 1).

[12] The off-axis TOBI data show significant asymmetry between the two ridge flanks over the past 3 Ma. To the north, although now dismem-

bered by numerous small to medium faults (throw and heave up to a few hundred meters), volcanic textures can still be identified, and the terrain is similar to parts of the Mid-Atlantic Ridge of similar age [Brace, 2003; Escartin *et al.*, 1999; Searle *et al.*, 1998a]. To the south, by contrast, faults have larger throws and heaves and hummocky volcanic terrain is patchy and relatively rare

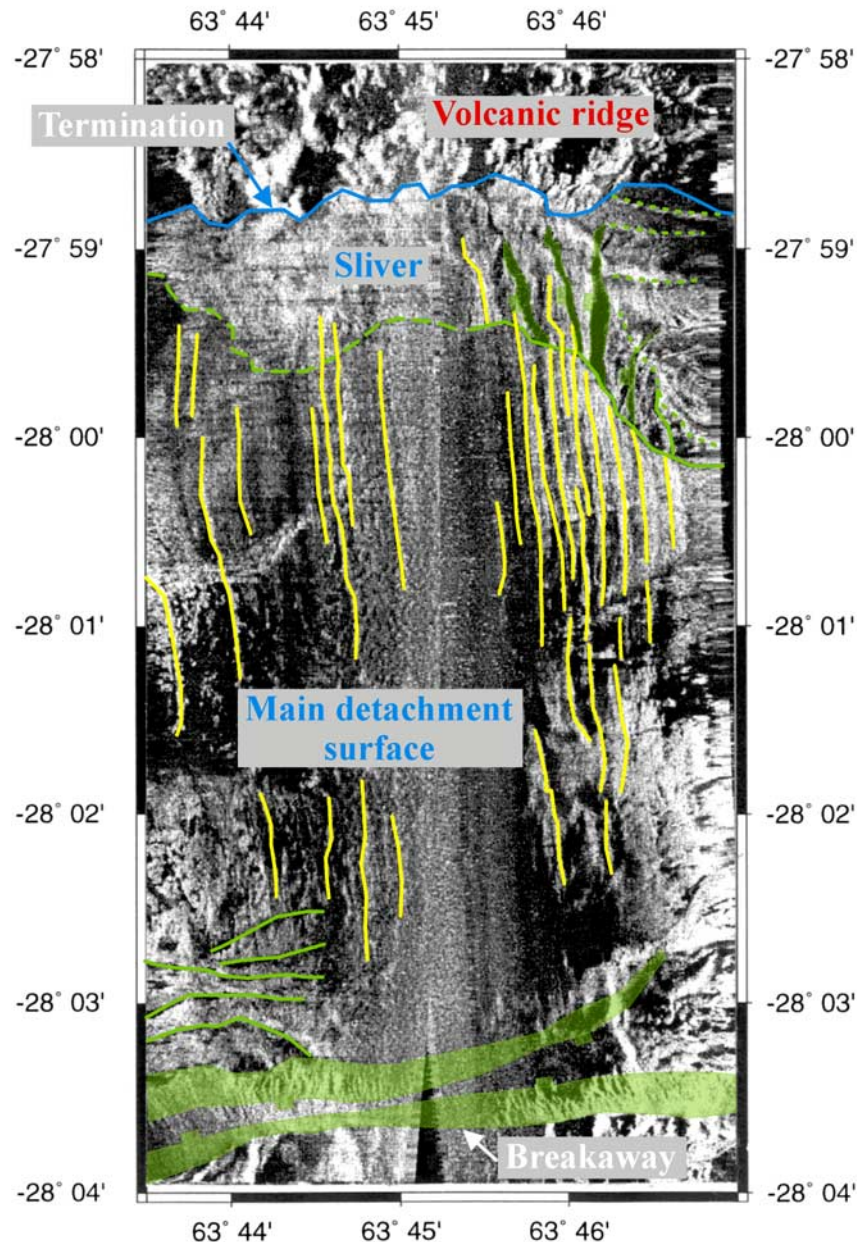


Figure 3. (continued)

[Bratee and Searle, 2001; Bratee, 2003]. Off-axis bathymetry and gravity data collected during the *Indoyo* cruise up to crustal ages of ~ 10 Ma [Cannat *et al.*, 2003] confirm that crustal accretion at this very slow spreading ridge leads to pronounced asymmetry, with dynamically supported shallow relief and thin crust on one plate, and deeper domains with thicker crust on the other plate. This is interpreted as due to large offset

asymmetric faulting of the crust in the axial valley domain [Cannat *et al.*, 2003].

4. FUJI Dome

[13] The FUJI Dome lies between 15 and 25 km south of the spreading axis (Figure 1). The *FUJI* multibeam bathymetry is too noisy to show the typical mullions of the detachment surface. How-

Table 1. Summary of Rock Samples

| Dive Number | Sample Number | Latitude, Degrees | Latitude, Minutes | Longitude, Degrees | Longitude, Minutes | Depth, Meters | Rock Type |
|-------------|---------------|-------------------|-------------------|--------------------|--------------------|---------------|------------------------------|
| 444 | 1 | 28 | 3.63 | 63 | 45.21 | 2699 | basalt |
| 444 | 2 | 28 | 3.63 | 63 | 45.21 | 2699 | basalt |
| 444 | 3 | 28 | 3.63 | 63 | 45.21 | 2699 | basalt |
| 444 | 4 | 28 | 3.63 | 63 | 45.21 | 2699 | basalt |
| 444 | 5 | 28 | 3.63 | 63 | 45.21 | 2699 | basalt |
| 444 | 6 | 28 | 3.34 | 63 | 45.27 | 2795 | basalt |
| 444 | 7 | 28 | 3.34 | 63 | 45.27 | 2795 | basalt |
| 444 | 8A | 28 | 3.34 | 63 | 45.27 | 2795 | basalt |
| 444 | 8B | 28 | 3.34 | 63 | 45.27 | 2795 | basalt |
| 444 | 9 | 28 | 3.34 | 63 | 45.27 | 2795 | basalt |
| 444 | 10 | 28 | 3.34 | 63 | 45.27 | 2795 | basalt |
| 444 | 11 | 28 | 3.27 | 63 | 45.26 | 2707 | basalt |
| 444 | 12 | 28 | 3.27 | 63 | 45.26 | 2707 | basalt |
| 444 | 13 | 28 | 3.27 | 63 | 45.26 | 2707 | basalt |
| 444 | 14 | 28 | 3.27 | 63 | 45.26 | 2707 | basalt |
| 444 | 15 | 28 | 3.27 | 63 | 45.26 | 2707 | basalt |
| 444 | 16 | 28 | 3.09 | 63 | 45.21 | 2545 | glassy breccia |
| 444 | 17 | 28 | 3.09 | 63 | 45.21 | 2545 | glassy breccia |
| 444 | 18 | 28 | 3.09 | 63 | 45.21 | 2545 | glassy breccia |
| 444 | 19 | 28 | 3.09 | 63 | 45.21 | 2545 | glassy breccia |
| 444 | 20 | 28 | 3.09 | 63 | 45.21 | 2545 | glassy breccia |
| 444 | 21 | 28 | 3.88 | 63 | 45.06 | 2431 | microtroctolite |
| 444 | 22 | 28 | 3.88 | 63 | 45.06 | 2431 | basalt |
| 444 | 23 | 28 | 3.88 | 63 | 45.06 | 2431 | microgabbro |
| 444 | 24 | 28 | 3.88 | 63 | 45.06 | 2431 | microgabbro |
| 444 | 25 | 28 | 3.88 | 63 | 45.06 | 2431 | basalt |
| 445 | 1 | 27 | 58.74 | 63 | 45.55 | 3982 | basalt |
| 445 | 2 | 27 | 58.74 | 63 | 45.55 | 3982 | basalt |
| 445 | 3 | 27 | 59.12 | 63 | 45.58 | 3940 | basalt |
| 445 | 4 | 27 | 59.12 | 63 | 45.58 | 3940 | metabasalt |
| 445 | 5 | 27 | 59.32 | 63 | 45.85 | 3816 | metabasalt |
| 445 | 6 | 27 | 59.32 | 63 | 45.85 | 3816 | metabasalt |
| 445 | 7 | 27 | 59.42 | 63 | 45.90 | 3752 | metabasalt |
| 445 | 8 | 27 | 59.42 | 63 | 45.90 | 3752 | metabasalt |
| 445 | 9 | 27 | 59.59 | 63 | 45.82 | 3731 | metabasalt |
| 445 | 10 | 27 | 59.62 | 63 | 45.83 | 3727 | metabasalt |
| 445 | 11 | 27 | 59.67 | 63 | 45.87 | 3680 | metabasalt |
| 450 | 1 | 28 | 0.06 | 63 | 46.16 | 3416 | basalt |
| 450 | 2 | 28 | 0.70 | 63 | 45.87 | 3273 | basalt |
| 450 | 3 | 28 | 0.73 | 63 | 45.74 | 3193 | basalt |
| 450 | 4 | 28 | 0.77 | 63 | 45.56 | 3097 | basalt |
| 450 | 5 | 28 | 0.80 | 63 | 45.43 | 3048 | basalt |
| 450 | 6 | 28 | 1.06 | 63 | 45.42 | 2965 | basalt |
| 450 | 7 | 28 | 1.21 | 63 | 45.48 | 2923 | Foraminiferal ooze |
| 450 | 8 | 28 | 1.41 | 63 | 45.67 | 2869 | serpentinised harzburgite |
| 450 | 9 | 28 | 1.54 | 63 | 45.83 | 2867 | basalt |
| 450 | 10 | 28 | 1.68 | 63 | 46.05 | 2866 | basalt |
| 450 | 11 | 28 | 1.70 | 63 | 46.08 | 2863 | basalt |

ever, they have been combined with the better data from the *Indoyo* cruise which exist east of $63^{\circ}39'E$ at the latitude of the detachment, and these latter data do show clear mullions (Figure 1). Note,

however, that there are a number of N-S (track-parallel) artifacts in Figure 1, which must be carefully distinguished from true mullions. Off-axis bathymetry and gravity data collected during

Table 2. Seafloor Gravity Data

| Dive-Station Number | Latitude, Degrees S | Longitude, Degrees E | Depth, m | Observed Gravity, mGal | Terrain Correction mGal | Residual Bouguer Anomaly ^a , mGal |
|---------------------|---------------------|----------------------|----------|------------------------|-------------------------|--|
| 444-6 | 28.0477 | 63.7501 | 2427 | 979804.25 | 44.9 | 0.0 |
| 445-2 | 27.9812 | 63.7572 | 4004 | 980048.02 | 13.1 | 1.2 |
| 450-5 | 28.01342 | 63.7593 | 3050 | 979911.60 | 30.4 | -22.6 |

^aRelative to station 444-6.

the *Indoyo* cruise show that the FUJI Dome is one of the dynamically supported massifs identified in the area [Cannat *et al.*, 2003], yet it seems to be the only one that bears the characteristic corrugations of a megamullion.

[14] On the basis of TOBI side scan data, the FUJI Dome detachment appears to extend at least 18 km along strike and up to 8 km across strike in what we interpret as a completely exposed single detachment surface (Figure 2). The eastern end coincides with a “turtle-back” dome 15 km long, 10 km wide and 1500 m high such as is characteristic of detachments at the MAR and on continents [Tucholke *et al.*, 1997]. Here the detachment is characterized by a smooth-looking surface with strong N-S lineations visible in the side-scan image, cross-cut in places by minor faulting, and bounded to north and south by sharply-edged blocks of volcanic terrain (Figures 2 and 3).

[15] On the basis of the side scan image, the smooth surface continues west to about 63°37'E, with further N-S lineations near 63°40'E. To the north, south and east the detachment is bounded by typical hummocky volcanic terrain, but in the west it merges into what has elsewhere been called “basement” terrain and has been suggested to be lower crust or upper mantle [Blackman *et al.*, 1998; Cann *et al.*, 1997; Parson *et al.*, 2000]. This terrain is characterized by short, curving lineaments with a variety of trends, and showing both strong reflections and narrow shadows, suggesting steep ridges and valleys or scarps.

[16] Our interpretation of the western edge of the detachment (Figure 2) places it part way along a second, smaller topographic dome centered at 63°36'E). Oceanic detachments are commonly associated with pairs of domes along strike [MacLeod *et al.*, 2002; Tucholke *et al.*, 2001], so

we carefully examined this second dome to see if it is an integral part of the detachment. Its crest is poorly imaged under TOBI's nadir, but its western flank is certainly characterized by the typical “basement” terrain and does not have spreading-parallel striations (Figure 3).

[17] The surfaces of most oceanic megamullions appear to be truncated by a ridge or series of ridges and valleys inferred to coincide with the breakaway - i.e., the point on the footwall where the detachment begins [e.g., MacLeod *et al.*, 2002; Ranero and Reston, 1999; Reston *et al.*, 2002; Tucholke *et al.*, 1998a; Tucholke *et al.*, 2001]. In the model of Tucholke *et al.* [1998a], the breakaway is at a normal fault which subsequently continued slipping for much longer than usual. Lavier *et al.* [1999]'s numerical model shows that the lithosphere below the detachment rotates significantly away from the ridge, producing an upstanding dome, with the top of the initial normal fault becoming a sharp ridge on the older side of the dome having a steep slope facing the spreading axis. The FUJI Dome has a similar shape to these other observed and modeled detachments, with the broad dome bounded to the south by a sharp valley and ridge (Figures 1, 2a, and 4). The valley axis is at 28°03.5'S in the region of our dives at 63°45'E (Figure 3a), and the side scan suggests that its southern flank is a north-facing normal fault, whose top (at 28°03.6'S) we interpret as the breakaway. A bathymetric profile through the FUJI Dome (Figure 4) suggests the possibility of the breakaway being at the crest of the small ridge at 28°05.5'S (-28.09°) rather than 28°03.6'S as suggested above. We cannot completely rule out this interpretation, but we favor the more northerly position because both the shaded bathymetry and the TOBI side scan suggest that the 28°03.5'S valley is the southern

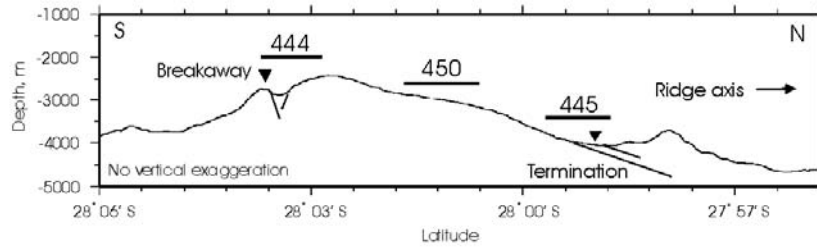


Figure 4. North-South topographic cross-section through the FUJI detachment, showing the approximate positions of the dives and inferred sub-surface fault planes.

boundary of the mullion structures and striations (Figures 1 and 2). The short, closely-spaced, roughly N-S lineaments associated with the two normal fault scarps flanking this valley are features such as spurs, gulleys and talus chutes associated with mass wasting of the scarps, such as have been clearly imaged by TOBI on numerous normal fault scarps not associated with detachments [Allerton *et al.*, 1995; McAllister and Cann, 1996; Searle *et al.*, 1998a]. Immediately south of the 28°03.5'S valley, TOBI shows a large expanse of hummocky volcanic seafloor extending as far south as 28°05'S. If the breakaway is at 28°05.5'S, then this must represent a large allocthonous block riding above it.

[18] The youngest point on the detachment surface, where it ceases to slip and touches the top of the hanging wall, is called the termination. We interpret this as the clear boundary between the flat, lineated terrain of the detachment, and the hummocky volcanic terrain to its north (Figures 2 and 3c). This boundary lies at the foot of a shallow E-W valley at 27°59'S in the region of Figure 3.

5. Magnetics

[19] Total magnetic field anomalies (reduced to IGRF) from the *Indoyo* cruise show a clear central anomaly and anomalies 3A (approximately 6 Ma) and 5 (approximately 10 Ma) [Bralee and Searle, 2001; Bralee, 2003; Searle and Bralee, 2001]. These anomalies are generally well-correlated along the length of the segment and fit an average half spreading rate of about 7 km Ma⁻¹. Between these a number of peaks and troughs can be seen

but are harder to correlate along strike (particularly on the Antarctic flank) and to date. Note that for this N-S spreading ridge, positive anomalies form over the northern and negative anomalies over the southern boundaries of normally magnetized blocks.

[20] Figure 5 shows a N-S magnetic anomaly profile at 63°45'E, together with two simple models. A small, positive magnetic anomaly occurs over the FUJI Dome, peaking about 21 km south of the axis (near 28°02'S). This is continuous with similar anomalies on several profiles away from the detachment toward the segment centre [Bralee and Searle, 2001; Bralee, 2003; Searle and Bralee, 2001]. We interpret this as the positive anomaly over the young edge of Chron 2n (see below). Its existence here indicates that the lithosphere beneath the detachment was being magnetized as it was unroofed. Depending on the precise lithology of the footwall, this presumably occurred by thermal remanent magnetization of gabbro or peridotite as they cooled during uplift, or by chemical remanent magnetization of peridotite during serpentinization.

[21] The first model (Figure 5a) is for a constant spreading rate of 7 km Ma⁻¹. This model gives a small positive anomaly near chron C2n as identified above. A similar positive anomaly is predicted over the old edge of C2n on the north flank, about 25 km north of the axis. These modeled peaks are close to the observed peaks, but for this constant spreading rate model they lie slightly to the north of each. The second model (Figure 5b) assumes that from 2.58 Ma (the age of the breakaway on this model) until 1.95 Ma (the age of the termina-

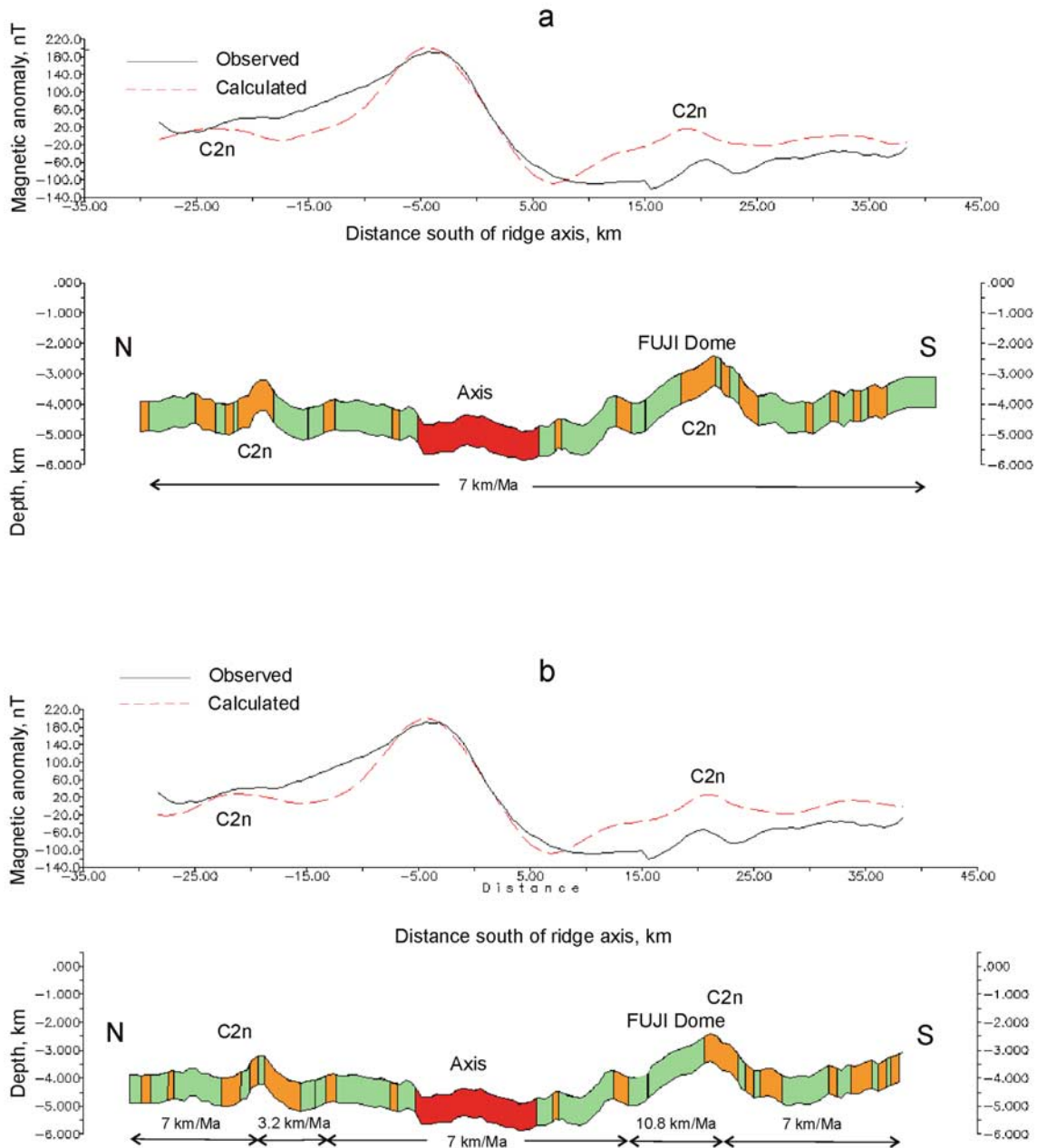


Figure 5. Total magnetic field anomalies from *Indoyo* cruise (solid black lines), with calculated anomalies (broken red lines) for the models shown below. (a) Constant spreading rate of 7 km Ma^{-1} throughout. Source thickness is 1 km ; magnetizations are remanent only, 5 A m^{-1} for Brunhes ($0\text{--}0.78 \text{ Ma}$) and $\pm 0.5 \text{ A m}^{-1}$ for other bodies: red/orange, normal magnetization; green, reversed. (b) Same as Figure 5a, except that for the interval 2.58 Ma (the age of the breakaway on this model) until 1.95 Ma (the age of the termination) there is reduced crustal accretion on the northern (African) flank at 3.2 km Ma^{-1} , and the rest of the plate separation is taken up by slip at 10.8 km Ma^{-1} on the FUJI Dome detachment, accompanied by magnetization of the footwall as slip occurred. Horizontal axis gives distance north or south of the current spreading axis. Anomaly 2n is labeled.

tion), most of the plate separation was taken up by slip on the detachment at 10.8 km Ma^{-1} , while reduced magmatic accretion at 3.2 km Ma^{-1}) occurred on the African plate. However, consider-

ing the generally poor fidelity with which magnetic anomalies on the Southwest Indian Ridge record field reversals, we should not rely too much on the precise details of this model.

[22] Both models in Figure 5 require a strong off-axis attenuation of magnetization, from 5 A m^{-1} for the Brunhes (0–0.7 Ma) to 0.5 A m^{-1} elsewhere. This applies to the whole of both modeled flanks, not just FUJI Dome. The models also generally over predict the amplitude on the south flank between 8 km and 38 km south of the axis, and under predict it on the north flank between -7 km and -28 km . We have not been able to match these amplitude variations by varying the magnetization in the simple blocks of these models, including reduced (and zero) magnetization under FUJI Dome.

6. Gravity

[23] The Residual Mantle Bouguer Anomaly (RMBA) was calculated from *Indoyo* data using the method of *Parker* [1972] and *Kuo and Forsyth* [1988], assuming water, crustal and mantle densities of 1030 , 2700 and 3300 kg m^{-3} , respectively and a crustal thickness of 7 km [*Brale*, 2003; *Searle and Brale*, 2001]. Use of a multi-layer crust does not significantly change the shape of the anomaly.

[24] Figure 6 shows a N-S profile of the RMBA at $63^{\circ}45'E$. This exhibits a regional increase of some 40 mGal from the ridge axis near $27^{\circ}55'S$ to the flank around $28^{\circ}10'S$ which does not occur on the north flank of the ridge, and is not a result of the axial thermal anomaly, which has been accounted for. We attribute it to asymmetric crustal accretion, with crust on average about 2 km thicker on the north flank than the south flank [*Brale*, 2003; *Cannat et al.*, 2003; *Searle and Brale*, 2001]. Superimposed on this regional trend is a peak of about 30 mGal situated over FUJI Dome. The gradients on the flanks of this anomaly are about 2.9 mGal km^{-1} to the north and 4.0 mGal km^{-1} to the south. This anomaly is about 50% larger, and the gradients more than double, those reported over Dante's Domes, (20 mGal and 1.3 mGal km^{-1} , [*Tucholke et al.*, 2001]).

[25] The seafloor gravity data were calculated using the methodology of *Luyendyk* [1984] and *Tucholke et al.* [2001]. The Fourier transform method used to calculate the sea-surface RMBA

results in the anomaly having an arbitrary datum, so its absolute difference from the seafloor anomaly is unknown. In Figure 6 the three seafloor anomalies are plotted with their mean matching the mean of the corresponding sea surface values. In modeling the gravity, we have therefore attempted to match the shape and gradients of both the sea surface and the seafloor anomalies, but not their absolute values.

[26] The seafloor anomalies reflect the gravity peak seen in the sea surface data, but with steeper flanks, as was also found at Dante's Domes on the northern Mid-Atlantic Ridge [*Tucholke et al.*, 2001]. Observational errors are estimated at approximately 0.5 mGal , and the only other large error, in the terrain correction, is estimated at a maximum of about 2 mGal for the station on dive 444. These data yield a maximum gradient of 7 mGal km^{-1} to the north between stations 450-5 and 445-2, compared to approximately 3 mGal km^{-1} on both flanks of Dante's Domes. The Bouguer anomalies at stations 444-6 and 450-5 are very similar; we did not make a measurement far enough south to see if there is a strong gradient away from the dome crest as at Dante's Domes.

[27] We have modeled both the sea-surface and seafloor Bouguer anomalies. Since we lack additional constraints (e.g., seismic) or extensive seafloor gravity observations, we have avoided seeking detailed "best fit" models, and instead use the modeling to provide some constraints on generic models. This allows us to make a number of fairly robust statements:

[28] 1. First, there must be substantially thinner or denser than normal crust under the FUJI Dome. A model such as *Tucholke et al.* [2001] derived for Dante's Domes, in which gabbro outcrops across the Dome and the moho is raised 1 km except for a narrow peridotite dome grossly underestimate the observed sea-surface gravity (maximum misfit 15 mGal).

[29] 2. On the other hand, uniformly outcropping, unserpentinized peridotite across the Dome significantly overestimates the sea-surface gravity by about 15 mGal .

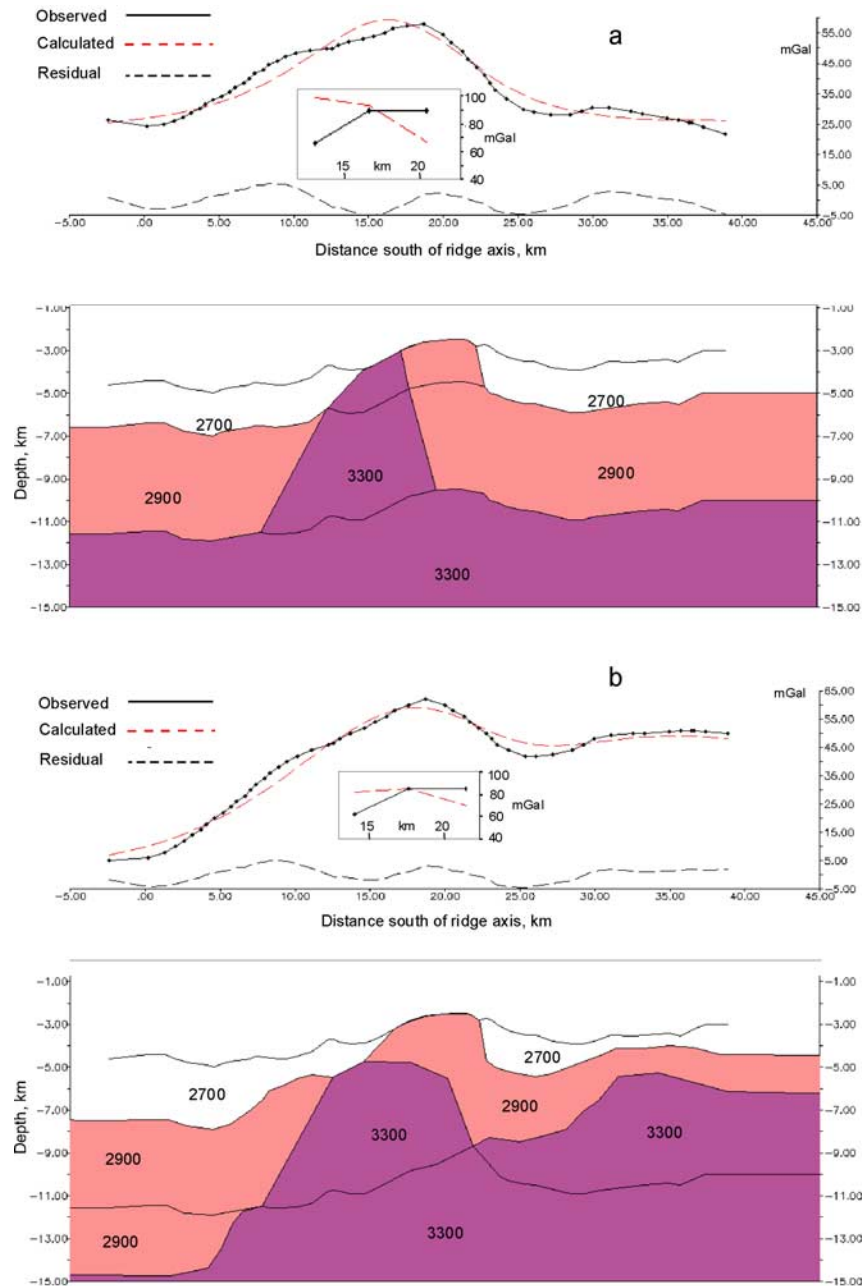


Figure 6. (a) N-S profile of residual Bouguer gravity anomaly over the FUJI Dome at $63^{\circ}45'E$. Upper solid line: Residual Mantle Bouguer Anomaly calculated from *Indoyo* shipboard data using the method of *Parker* [1972] and *Kuo and Forsyth* [1988], assuming water, crustal and mantle densities of 1030 , 2700 and 3300 kg m^{-3} , respectively and a crustal thickness of 7 km . A linear regional gradient of $0.55 \text{ mGal km}^{-1}$ down to the north has been removed. Inset: RMBA calculated from seafloor gravity observations made in the submersible *Shinkai 6500* using the method of *Luyendyk* [1984] and *Tucholke et al.* [2001], with terrain corrections out to Hammer zone M (21.9 km) [*Hammer*, 1939], after setting the mean of observed and calculated anomalies equal. The absolute difference between the shipboard and seafloor RMBA is uncertain because of the arbitrary datum involved in the Fourier transform calculation used in the shipboard case, so the absolute values of the gravity scales are arbitrary. Dashed red lines: Bouguer anomaly calculated from the crustal density model shown below, which is based on the structure obtained by numerical modeling of *Lavier et al.* [1999]. (b) Observed sea-surface RMBA (with no regional removed) and an approximation to a “best fit” model achieved by setting an approximately uniform upper layer to the Dome, and adjusting the lateral boundaries of the 3300 kg m^{-3} body to fit the anomaly over the Dome, and the crustal thickness to match the regional gradient. Inset shows seafloor data as for Figure 6a. See text for further details.

[30] 3. The observed seafloor gravity gradients are not consistent with any model that has substantial shallow horizontal density contrasts on the Dome (e.g., juxtaposed gabbro against either peridotite or basalt), although such models can reproduce our observed sea surface gravity anomalies.

[31] 4. Without the help of further constraints on crustal thickness and density, it is difficult to constrain the dip of the buried detachment north of the termination.

[32] We explored a number of gravity models based on the structure obtained in the final step of the numerical modeling of *Lavier et al.* [1999] (Figure 6a). These models assume a layered crust with 2 km of basalt/diorite (density 2700 kg m^{-3}) overlying 5 km of gabbro (density 2900 kg m^{-3}) with a peridotite mantle of density 3300 kg m^{-3} . In *Lavier et al.* [1999]'s model, slip on the detachment combined with isostatic forces and bending moments cause the footwall to rise and bend upward, tilting outward, away from the ridge axis. As it does so, a wedge of mantle rises beneath it. We modeled this by tilting the 2700 kg m^{-3} and 2900 kg m^{-3} crustal layers up under the southern part of the Dome and breakaway region, and replacing them by a 3300 kg m^{-3} wedge under its northern part. Models such as this (e.g., Figure 6a) can provide a good fit to the sea-surface data, but because of the shallow lateral density contrasts they do not fit the seafloor data well (maximum misfit 28 mGal for model in Figure 6a). The model in Figure 6a assumes the breakaway is at $28^{\circ}3.5'S$. If we place the breakaway, and thus the outcrop of the gabbro-peridotite contact, farther south, then the seafloor data can be well fitted but the sea surface anomaly is overestimated because now the whole of the dome is underlain by peridotite. Figure 6b shows an approximation to a "best fit" model. This model is loosely based on that of Figure 6a, but has a more extensive, approximately 2 km thick, 2900 kg km^{-3} layer over the dome to try to fit the seafloor gradients. We then adjusted the lateral extent of the 3300 kg m^{-3} body to best fit the seafloor data over the Dome, and finally adjusted the crustal thickness to approximately match the regional gradient. The calculated and observed

sea-surface anomalies are everywhere within ± 5 mGal of each other. After adjusting the mean of the observed seafloor anomaly to the mean of the calculated anomaly, the maximum misfit in the seafloor data is 19 mGal. The fit could doubtless be improved by ad-hoc adjustments to the layer densities and thicknesses. While recognizing that this, as any gravity model, is highly non-unique, we suggest that it illustrates the major features of the density distribution that must exist here, i.e., a crust thinning from north to south, a high density intrusion under the dome (which is therefore at least partly dynamically supported), and a fairly constant density lithology in its upper part.

[33] We cannot directly infer lithology from the model densities. Although densities of 2700 kg m^{-3} , 2900 kg m^{-3} , and 3300 kg m^{-3} would be appropriate for basalt, gabbro and peridotite, respectively, it is important to remember that serpentinized peridotite can have significantly lower density, depending on the degree of serpentinization, and may have similar density to gabbro. We also recognize that, at this segment-end location on a very slow spreading ridge, the "crust" may well not have a simply layered structure but could be a quite heterogeneous mixture of gabbro and peridotite with varying degrees of serpentinization [*Cannat*, 1996].

7. Submersible Dives

[34] The positions of the three dives conducted on the FUJI Dome (numbers 444, 445 and 450) are shown on Figure 3, and depth profiles of each dive, annotated with geological observations, are shown in Figure 7.

7.1. Detachment Boundaries

[35] The detachment surface represents a distinct formation that is different from those adjacent to it to the north and south. North of the termination (northern boundary of the Dome) there is a volcanic ridge (visited at the start of dive 445, Figure 7b) composed of moderately old but clearly identifiable pillow basalts and tubes,

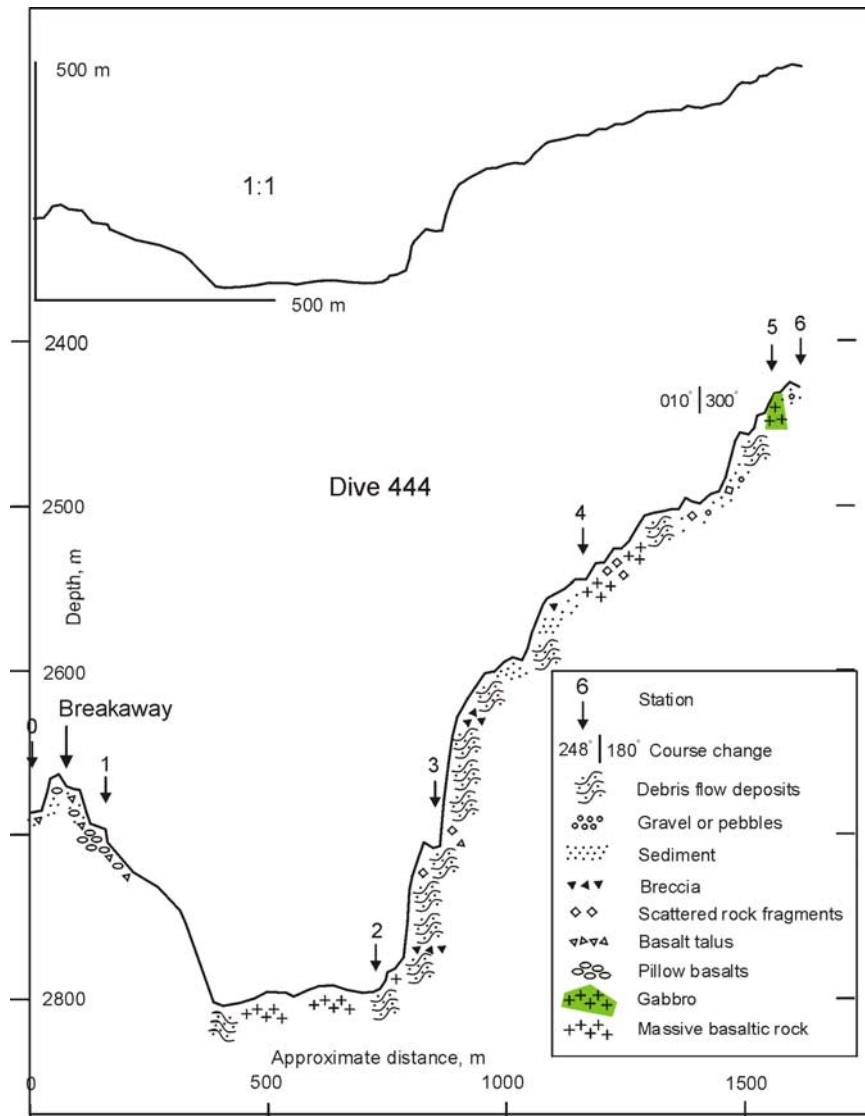


Figure 7. Depth profiles of dives (a) 444, (b) 445 and (c) 450, respectively, with geological interpretations and station positions. Station numbers correspond to circled numbers on Figure 3a. See Figure 3 for plan views of dive tracks.

many of which are unbroken and in situ. Sample 445-R1 from here is a piece of slightly altered aphyric basaltic lava tube (Table 1). This ridge has all the appearances of normal volcanic sea-floor. Generally, the orientations of the pillows indicate that only minor tilting has occurred since eruption. In one place, a large in situ drained pillow exposed drainage sills indicating that it has tilted about 10° to the south. No evidence was seen for more extreme tilts. The termination itself is marked by a narrow, sedimented valley

that separates the volcanic ridge to the north from the detachment surface to the south. No fault contact was visible.

[36] South of the detachment, on the ridge whose crest we interpret as the breakaway (visited on dive 444, Figure 7a), there are also intact and probably in situ pillows and tubes, although there is a slightly greater proportion of broken pillows and pillow talus than at the termination. The faulted northern flank of this ridge, which we interpret as

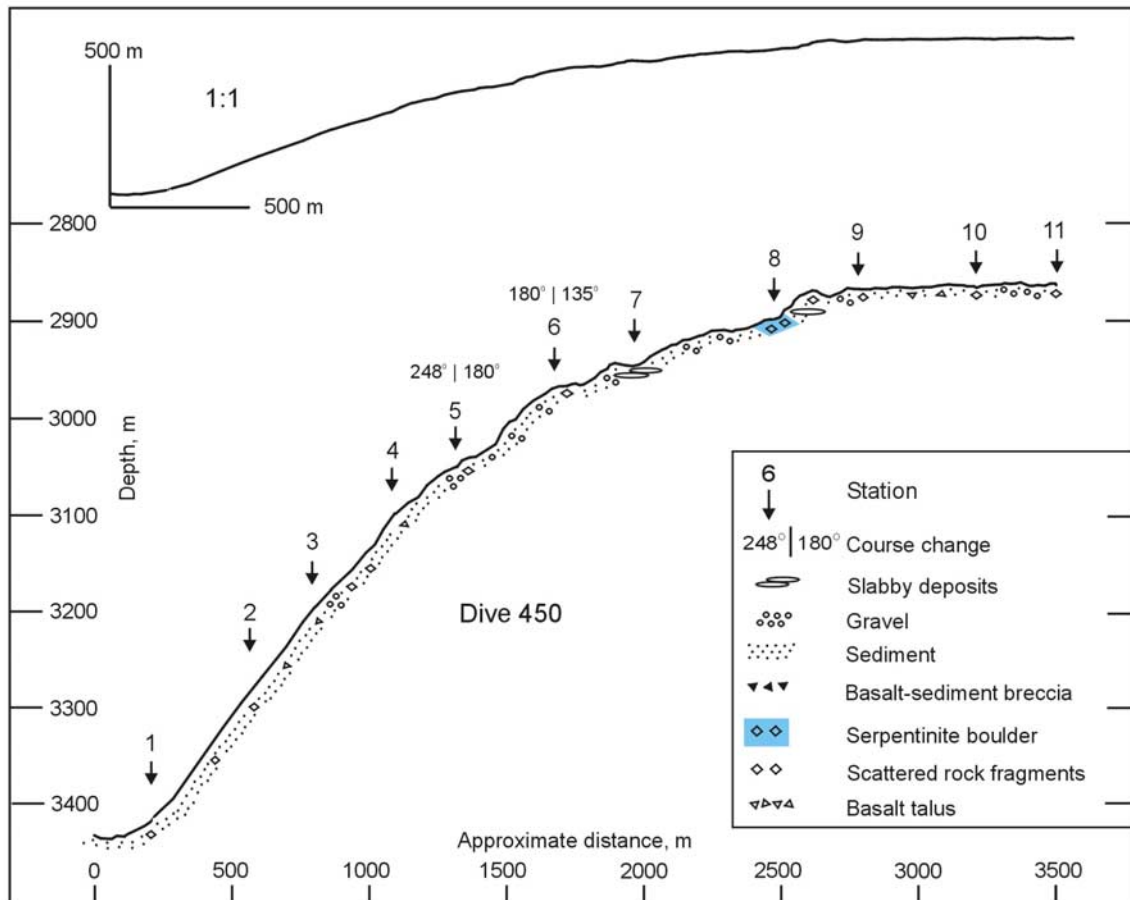
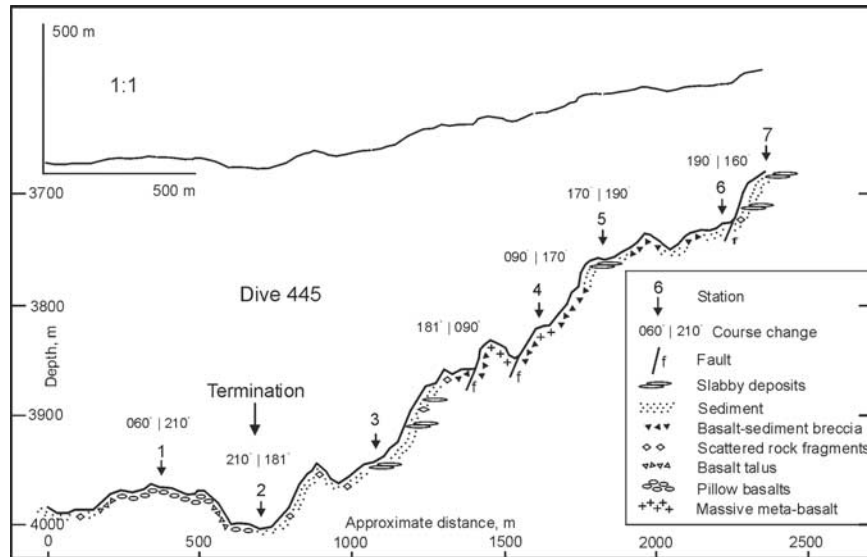


Figure 7. (continued)

the normal fault at which the detachment was initiated, was not examined.

7.2. Detachment Surface

7.2.1. Southern Slope (Dive 444)

[37] In terms of structure, the southern slope of the dome is a steep wall that appears to be a fault surface, at least near its foot: it dips at about 45° to the south, exposes some foliated or schistose rocks (unsampled) at its base, and just above these (2792 m, Figure 7a) has an apparent intrusive body whose upper surface is planar, dips 30° or more to the south and displays N-S oriented slickensides. At 2795 m, what appears to be a thin lava flow or sill dips 40° S, and nearby are some possible small dykes dipping about 30° N. If the sill and dykes were originally horizontal and vertical, respectively, they have been rotated 30° – 40° away from the ridge axis.

[38] Much of the steep south slope of the dome displays a groove-and-spur structure trending down slope with several meters of often sharp relief. We suggest that this corresponds to the localized striations seen on this fault scarp on the side scan image (Figure 3) and interpret it as a product of mass-wasting. Apart from the fairly rare, probably in situ rocks described above, the steep south slope is mostly covered by debris flow deposits (angular to rounded clasts of presumed igneous rock with varying proportions of sediment matrix from 0 to $>50\%$) which grade into semi-consolidated breccias, with occasional outcrops of more massive-looking rock, often fractured but some probably in situ (Figure 7a). Sampled clasts are aphyric and altered aphyric basalts (Table 1).

[39] The upper part of the south slope above 2600 m becomes less steep, with an increasing proportion of completely sedimented (often rippled) seafloor toward the summit of the dome (Figure 7a). Brecciated rocks continue between patches of sediment, and range between a) continuous, flat-lying surfaces of small, angular boulders, b) scattered deposits of mixed size, c) sometimes rounded boulders, and d) occasional very large (decametre) massive deposits. The latter were thought to be possibly in situ outcrops.

[40] Sampling of one massive outcrop at station 4 (2545 m, samples 444-R16 to 444-R20, Table 1) revealed a glassy breccia of welded fragments of pillow or other lava, while another near the summit (station 5, 2440 m, Figures 3, 7a) was revealed to be a breccia, from which altered aphyric basalt (444-R22), microtroctolite (444-R21) and microgabbro (444-R23, 444-R24), and a pale green mud, produced from the disaggregation of a metamorphosed mafic rock, were recovered. Most are slightly metamorphosed in the amphibolite to greenschist facies.

7.2.2. Northern Slope (Dives 445 and 450)

[41] With one exception (see below), the detachment surface north of the dome's summit has no clear-cut exposures of in situ hard rock. Overall sediment cover decreases (from a maximum of about 90% by area), and rubble cover increases, southward (up-slope) from the termination. On and in this sediment are two types of deposit. The first consists of closely spaced, poorly sorted rock clasts that range in size from coarse sand or gravel to large (>2 m) boulders. Sampled rocks were mostly variously altered basalts, although one was a serpentinized harzburgite (450-R08, 2899 m, Figures 3 and 7c). All are old with locally over 1 cm of manganese oxide crust, and none is in situ. No fault rocks (e.g., cataclasites) were found. The second type of deposit is flat and slabby, less than a meter high and extending several meters across. One of these was sampled and found to consist of a bed of manganese-coated, semi-indurated foraminiferal ooze (450-R7, Table 1). Typically both types of deposit are tens of meters across and separated from each other by tens to a few hundreds of meters. The edges of some of the rock deposits extend N-S, and they appear similar to the debris "fences" described from the Dante's Domes [Tucholke *et al.*, 2001]. It seems unlikely that such mass-wasting deposits would be sufficiently continuous to give rise to the striations seen on TOBI images, which are straight and coherent over many kilometers. However, we were unable to test this possibility fully. Most of the detachment surface north of the dome's summit is very smooth. We have no direct measurement of seafloor depth along the dives (submersible height above bottom

was not available) but plots of submersible depth against time for dive 450, when the submersible was maintaining an approximately constant height (within about ± 2 m) show apparent variations in depth of ~ 5 – 10 m amplitude and ~ 200 – 500 m wavelength superimposed on the regional slope. We suggest these variations may reflect depth variations across the spreading-parallel striations seen on TOBI, which have about the same wavelength, although our navigation is too imprecise to be able to match individual features from the depth profile to the side scan image.

7.3. Minor Faulting (Dive 445)

[42] Three small west-dipping fault scarps were imaged on the north-eastern corner of the detachment by TOBI (dark lineaments around $27^{\circ}59.3'S$, $63^{\circ}46'E$ in Figure 3) and were targeted as likely places for in situ exposures. Dive 445 crossed the two eastern scarps at about 1400 m and 1600 m from the start of the dive (Figures 3 and 7b). These scarps are 20–25 m high and dip from 20° to vertical. They have no fresh talus below them and appear to be inactive. The centre one of the three exposed mainly a breccia of igneous clasts in a sediment matrix. We climbed the easternmost scarp and then followed it along strike to the south (Figure 3). It exposed a mixture of sediment-basalt breccia and massive igneous rocks. In the breccia (stations 5 and 6, samples 445-R07, 445-R09, 445-R10), the clasts are variously altered, metamorphosed (greenschist facies) and mildly tectonized basalts. Samples from one massive igneous outcrop (station 4, samples 445-R05 and 445-R06) were fractured meta-basalt (greenschist facies), with sample R05 derived from a pillow lava rim, although the pillowed nature of this deposit was not apparent to visual examination from the submersible. Just below station 4 an apparent igneous intrusive feature, possibly a small dyke, was seen but not sampled.

[43] There is no doubt that this part of the detachment surface, which displays N-S striations on TOBI, contains in-situ basalts. They appear old, and predate the N-S faulting, which cuts them. All are metamorphosed, possibly to greenschist facies,

unlike most of the rubble samples collected from the detachment surface. However, these basaltic outcrops are very different from the small volcanic cones erupted on the surface of Dante's Domes [Tucholke *et al.*, 2001], which we did not encounter on any of our dives.

[44] These basalts are the only outcrops of clearly in situ rock found on the detachment. However, it should be noted that this site is separated from the rest of the detachment by a subtle, curved lineament on TOBI (starting at $28^{\circ}00.1'S$ on the eastern edge of Figure 3b, curving NW along the southern edges of the three N-S faults). This probably marks the edge of a thin sliver parallel to the main detachment (an "excision" in the terms of Davis and Lister [1988]), so we cannot conclude that the in situ samples are characteristic of the rest of the detachment footwall. This sliver may have come from the footwall (in which case at least this part of the detachment is floored by basalt), or the hanging wall, in which case it tells us nothing about the main detachment. The fact that the N-S TOBI striations appear to continue through this curved lineament (Figure 3b) suggests that the sliver was intimately involved in the main detachment motion, but with the present data we cannot be entirely sure.

8. Discussion

[45] The FUJI Dome detachment is one of very few known examples outside the North Atlantic or from a cold or very slow-spreading ridge, and is also now one of the best imaged.

8.1. Corrugations and Striations

[46] Our multibeam bathymetry data show a grooved or "mullioned" surface, similar to examples from the MAR [Blackman *et al.*, 1998; Cann *et al.*, 1997; Fujiwara *et al.*, 2003; Reston *et al.*, 2002; Tucholke *et al.*, 1996; 1998a; Tucholke, 1997]. Cann *et al.* [1997] suggest that well-developed corrugations occur only on surfaces near ridge-transform intersections; our results are consistent with this. The FUJI Dome shows clear striations on TOBI side scan. On the basis of our

observations, these could be caused by striated rubble deposits (although they appear too long and continuous for this to be very likely), or by topographic variations in either the sediment surface or the sediment covered basement, or both (which we think most likely but are unable to completely verify with the present observations). However, they are not caused by alternating outcrop and sediment as suggested by *Cann et al.* [1997].

8.2. Lithological Structure

[47] Very little mid- or lower-crustal or mantle rock was recovered. The only possible in situ outcrops are of gabbro and microtroctolite, near the summit of the Dome, but given that they were recovered from a breccia, we cannot be entirely sure that their ultimate origin was near this site. It is possible, though we think unlikely, that they spalled off the hanging wall at some point in the detachment's development. The rest of the detachment surface is quite smooth, sedimented, and strewn with predominantly basaltic rubble. This is very similar to Dante's Domes [*Tucholke et al.*, 1998b]. However, the origin of this rubble is unclear. At other detachments it has usually been assumed to have spalled off the hanging wall or a klippe near the termination [*Tucholke et al.* [1998b]]. At FUJI Dome the areal density of this rubble increases southward away from the termination, suggesting either that it may not originate from the hanging wall or, if it does, that the rate of rubble formation has decreased over time. The steep southern slope of FUJI Dome makes an origin south of there (e.g., south of the breakaway) unlikely, as does the distance it would need to be transported along what was at best a shallow slope to the north. It is possible that some of the scattered deposits represent the remains of barely buried rocks that have disaggregated in situ, although some are clearly sitting on top of sediment. It is also possible that significant quantities of basalt outcrop near the summit of the dome. There is no evidence for this from TOBI side scan in the region of our dives (Figure 3), although we have identified areas of volcanic terrain on the detachment near 63°41'E and 63°48'E (Figure 2). We did not, however,

observe any of the small volcanic cones observed on Dante's Domes [*Tucholke et al.*, 2001].

[48] Dive 445 recovered the only other in situ rocks, which are metabasalts from what we interpret as a thin tectonic sliver or excision lying above the main detachment surface near the termination. The metamorphism suggests that the rocks, although containing pillow basalts, have been buried to some depth, in contrast to the basaltic rubble from the rest of the detachment surface which is all unmetamorphosed. This is consistent with the sliver having been unroofed by faulting parallel to the main detachment (Figure 4).

[49] Although we have few in situ samples, our gravity modeling suggests that dense and therefore probably lower crustal rocks (gabbro and/or serpentinitised peridotite) must be present near the surface of the Dome. We found decametre sized blocks near the summit of the dome, where we sample gabbro (dive 444). These large blocks are thought to be either in situ or else near their point of origin. Our recovery of a peridotite boulder implies an outcrop of peridotite also on the Dome.

[50] The general similarity to Dante's Domes suggests that this lithological structure may be a common feature of mid-ocean ridge detachments. However, it is not consistent with models [*Tucholke and Lin*, 1994] and observations from the Troodos ophiolite [*Varga and Moores*, 1990] where the detachment is at the dyke-gabbro boundary or exposes continuous gabbro [*Karson*, 1990]. We find frequent basaltic rubble and rare dykes, gabbro and serpentinite, but no evidence of a sheeted dyke formation. This perhaps suggests that rather than a "classical" layered crust at the detachment, basalts were erupted directly onto gabbro or even serpentinitised peridotite with little or no sheeted dyke layer, similar to the model of *Cannat et al.* [1995] for segment ends.

8.3. Tectonic Pattern

[51] Several models of core complexes [*Buck*, 1988; *Lister and Davis*, 1989] show the multiple, stacked normal fault blocks lying on the main

detachment with their fault planes dipping at shallow angles toward the termination. In these models, such fault blocks have been strongly rotated so that their originally horizontal surfaces are almost vertical. We have inferred the existence of a thin fault sliver near the breakaway (Figure 3). It is possible that this is analogous to such strongly rotated fault blocks, although we have no evidence to suggest the degree of rotation here.

[52] *Buck's* [1988] model shows that multiple faulting can weaken the lithosphere and so allow it to bend through large angles. In particular, his model predicts that the hanging wall may “roll over” so that its surface dips at large angles toward the footwall (i.e., to the south, away from the ridge axis). Our observations of the FUJI hanging wall suggest that it only dips about 10° to the south, within the usual range of outward dip of mid-ocean ridge normal fault blocks [Searle, 1992]. Of course it is possible that the lavas on which this observation is based were erupted quite late, *after* significant hanging wall rotation had occurred, but we see no evidence in either the side scan or bathymetry data that such was the case.

[53] The detachment itself dips at about 20° near the termination, a relatively shallow angle, like most other oceanic detachments. Our data are unable to constrain the dip below the hanging wall, where different models predict either continued low-angle dip e.g., [Dick *et al.*, 1991] or a transition to a steeply-dipping fault [e.g., Cann *et al.*, 1997; Tucholke *et al.*, 1998a]. There is some support for a low-angle model elsewhere from gravity [Blackman *et al.*, 1998] and seismic data [Ranero and Reston, 1999]. However, we are unable to constrain the subsurface dip at the FUJI Dome with the available data; in particular, our gravity data cannot constrain the dip without additional information on the crustal structure here.

[54] The south side of FUJI dome (like Dante's Domes) dips steeply ($\sim 45^\circ$) away from the ridge axis, so that it has probably flexed through an angle of over 50° during the full history of slip, and is locally down-faulted away from the ridge axis.

Most models of oceanic detachments suggest that the footwall will have been exhumed from near the ridge axis where the brittle-ductile transition may be quite shallow, resulting in a very thin elastic plate. The footwall may then flex easily in response to isostatic forces and bending moments so that its surface dips increasingly away from the ridge axis. Doming of the detachment surface might be enhanced by isostatic uplift following unloading [Lister and Davis, 1989], although the degree of unloading here may be insufficient, and it is not clear that this would lead to much larger outward dips on the breakaway side of the dome. However, MacLeod *et al.* [2002] have described a detachment on the MAR at $15^\circ 45'N$ where there is a well developed dome but no evidence of ductile deformation. They suggest that this detachment might root in a serpentinization front well above the brittle-ductile transition, which would presumably yield a much thicker footwall plate. Maximum hypocentral depths of microearthquakes [e.g., Wolfe *et al.*, 1995] and estimates of effective elastic thickness based on lithospheric flexure [e.g., Watts and Zhong, 2000] suggest a lithospheric thickness of 8–12 km at the axes of slow-spreading ridges. It may be therefore that in such cases some other mechanism such as extensive faulting reduces the effective elastic thickness sufficiently to allow such profound flexure.

[55] Low density plutons beneath a detachment (e.g., gabbro intruded into peridotite) can also cause doming [Yin, 1991]. MacLeod *et al.* [2002] and Escartin *et al.* [2003] found gabbro directly underlying the $15^\circ 45'N$ MAR detachment in an area of extensive peridotite. However, for such plutons to have sufficient buoyancy to drive the doming process, doming would have to occur before there was extensive serpentinization of the surrounding peridotite, implying that the latter would have to be quite a late-stage process. However, the existence of a positive Bouguer anomaly over FUJI Dome would seem to rule out the possibility of buoyancy-driven uplift here. Nevertheless, whether or not such plutons are sufficiently buoyant to drive or enhance uplift and doming, they may provide strong rheological contrasts. These would tend induce stress concentrations,

causing detachments to nucleate on the boundaries of the plutons. If the plutons are stronger than the surrounding peridotite, they could strengthen the footwall of large offset axial faults, and this might explain why megamullions are localized features whereas large offset faults appear to be almost ubiquitous in inside corner contexts.

[56] Finally, *Tucholke et al.* [1998a] have suggested that oceanic detachments are associated with a lowering in the melt delivery to, and magmatic accretion at, a ridge. We tested this by modeling magnetic anomalies over the FUJI Dome and its conjugate seafloor. Although the resolution of the sea-surface magnetic anomalies is limited, they are consistent with a model in which there is slip at more than the half spreading rate on the detachment, accompanied by diminished (though not zero) magmatic accretion on the conjugate flank. This model suggests that the duration of active slip on the detachment was about 1 Ma. Even so, the FUJI Dome carries magnetic anomalies that are continuous with those formed in presumed magmatically spread crust nearer the segment centre. This implies that, whatever the underlying lithology, it is capable of acquiring a remanent magnetization comparable to that of the normal magnetic source rocks.

9. Conclusions

[57] We have discovered and imaged a complete oceanic core complex and detachment surface on the very slow spreading (7 km Ma^{-1}) southwest Indian Ridge. The detachment is 20 km south of the ridge axis in the inside corner of a non-transform discontinuity. It is characterized by a 1500 m high ellipsoidal bathymetric dome (the FUJI Dome) and a detachment surface that is seen to be grooved or mullioned on shipboard multi-beam bathymetry and striated on deep-towed side-scan sonar. These striations do not reflect outcropping basement, but may be shallow topographic ridges and troughs. The detachment extends at least 18 km along-axis and about 8 km across axis.

[58] A positive magnetic lineation runs continuously through the feature and is continuous with

the same anomaly outside the detachment at the segment centre, indicating that the lithosphere beneath the detachment was being magnetized during its formation. We interpret this anomaly as the young end of anomaly 2A (approximately 2.6 Ma). Sea-surface magnetic anomalies have poor resolving power at this slow spreading rate, but modeling conjugate anomalies on both flanks suggests that during active slip on the detachment, crustal extension was asymmetric, with faster accretion at about 10.8 km Ma^{-1} on the south flank (via tectonic extension on the detachment), with slower than normal (3.2 km Ma^{-1}) magmatic accretion on the north flank. The modeling suggests that the detachment was active for about 1 Ma.

[59] Three submersible dives were conducted on the Dome. They confirmed apparently *in-situ* volcanic seafloor, with only minor tilting, immediately north and south of the detachment surface. The south flank of the Dome dips steeply, up to 45° away from the ridge axis, with evidence of 30° – 40° outward rotation, is characterized by extensive breccia and mass-wasting deposits, and is locally down faulted to the south. The northern flank dips gently (about 11°) to the north and is covered by sediment and mostly basaltic rubble. Near the termination a thin sliver appears to lie above the main detachment and is locally broken by minor normal faults. Sampling these fault scarps recovered *in situ* meta-basalts and basaltic breccias. Our only recoveries of plutonic rocks were samples of apparently *in situ* gabbro near the crest of the Dome and a single serpentinite boulder from the northern flank.

[60] Sea-surface gravity anomalies show that the detachment is underlain by thinned or increased density crust. Seafloor gravity measured at three points on the detachment surface rule out extensive lateral, shallow density variations, such as basalt-gabbro or gabbro-peridotite contacts. Because of this, we have to rule out models in which a simple layered crust is strongly up warped beneath the Dome with layer 2/3 or Moho contacts occurring near the surface. In general, the gravity best fits a model of the Dome in which the basaltic crust is virtually absent, with gabbro

replacing normal layer 2 and peridotite replacing layer 3.

Acknowledgments

[61] The FUJI cruise was funded via InterRidge Japan, the European Union, the Natural Environment Research Council and the Centre National pour Recherche Scientifique. The INDOYO cruise was funded by the Japan Marine Science and Technology institute (JAMSTEC). Additional funding was provided by the University of Durham. We thank the officers and crew of N/O *Marion Dufresne* and the R/V *Yokosuka*, the pilots of the submersible *Shinkai 6500*, and the rest of the shipboard parties for their help. We are indebted to Daniel Sauter and two anonymous referees, whose thorough reviews resulted in considerable improvements to this paper.

References

- Allerton, S., B. J. Murton, R. C. Searle, and M. Jones, Extensional faulting and segmentation of the Mid-Atlantic Ridge north of the Kane fracture zone (24°00'N to 24°40'N), *Mar. Geophys. Res.*, *17*, 37–61, 1995.
- Blackman, D. K., J. R. Cann, B. Janssen, and D. K. Smith, Origin of extensional core complexes: Evidence from the Mid-Atlantic Ridge at Atlantis Fracture Zone, *J. Geophys. Res.*, *103*, 21,315–321,333, 1998.
- Braleo, A. V., A detailed geophysical study of the ultra-slow spreading Southwest Indian Ridge: The axis of segment 11 near 64°E, Ph.D. thesis, Dept. of Geol. Sci., Univ. of Durham, UK, 2003.
- Braleo, A. V., and R. C. Searle, Fault characteristics and strain accommodation at the ultra slow spreading southwest Indian Ridge (SWIR), *Eos Trans. AGU*, *82*(47), Fall Meet. Suppl., F1096, 2001.
- Buck, W. R., Flexural rotation of normal faults, *Tectonics*, *7*, 959–973, 1988.
- Cann, J. R., D. K. Blackman, D. K. Smith, E. McAllister, B. Janssen, S. Mello, E. Avgarinos, A. R. Pascoe, and J. Escartin, Corrugated slip surfaces formed at ridge-transform intersections on the Mid Atlantic Ridge, *Nature*, *385*, 329–332, 1997.
- Cannat, M., How thick is the magmatic crust at slow-spreading mid-ocean ridges?, *J. Geophys. Res.*, *101*, 2847–2857, 1996.
- Cannat, M., and J. F. Casey, An ultramafic lift at the Mid-Atlantic Ridge: Successive stages of magmatism in serpentinized peridotites from the 15°N region, in *Mantle and Lower Crust Exposed in Oceanic Ridges and in Ophiolites*, edited by R. L. M. Vissers and A. Nicolas, pp. 5–34, Kluwer Acad., Norwell, Mass., 1995.
- Cannat, M., et al., Thin crust, ultramafic exposures, and rugged faulting patterns at Mid-Atlantic Ridge (22°–24°N), *Geology*, *23*, 49–52, 1995.
- Cannat, M., C. Rommevaux-Jestin, and H. Fujimoto, Melt supply variations to a magma-poor ultra-slow spreading ridge (Southwest Indian Ridge 61° to 69°E), *Geochem. Geophys. Geosyst.*, doi:10.1029/2002GC000480, in press, 2003.
- Davis, G. H., A shear-zone model for the structural evolution of metamorphic core complexes in southeastern Arizona, in *Continental Extensional Tectonics*, edited by M. P. Coward, J. F. Dewey, and P. L. Hancock, *Geol. Soc. Spec. Publ.*, *28*, 247–266, 1987.
- Davis, G., and G. Lister, Detachment faulting in continental extension: Perspectives from the southwestern US Cordillera, *Spec. Pap. Geol. Soc. Am.*, *218*, 133–159, 1988.
- Dick, H. J. B., P. S. Meyer, S. Bloomer, D. Stakes, and C. Mawer, Lithostratigraphic evolution of an in situ section of oceanic layer 3, *Proc. Ocean Drill. Program Sci. Results*, *118*, 439–538, 1991.
- Escartin, J., P. A. Cowie, R. C. Searle, S. Allerton, N. C. Mitchell, C. J. MacLeod, and P. A. Sloomweg, Quantifying tectonic strain and magmatic accretion at a slow-spreading ridge segment, Mid-Atlantic Ridge, 29°N, *J. Geophys. Res.*, *104*, 40421–410,437, 1999.
- Escartin, J., C. Mével, C. J. MacLeod, and A. M. McCaig, Constraints on deformation conditions and the origin of oceanic detachments: The Mid-Atlantic Ridge core complex at 15°45'N, *Geochem. Geophys. Geosyst.*, doi:10.1029/2002GC000472, in press, 2003.
- Flewelling, C., N. Millard and I. Rouse, TOBI, a vehicle for deep ocean survey, *Elec. Comm. Eng. J.*, 85–93, 1993.
- Fujimoto, H., et al., Preliminary results from the first submersible dives on the Southwest Indian Ridge, *Eos Trans. AGU*, *79*(46), Fall Meet. Suppl., F893, 1998.
- Fujimoto, H., et al., First Submersible Investigations of the mid-ocean ridges in the Indian Ocean, *InterRidge News*, *8*, 22–24, 1999.
- Fujiwara, T., J. Lin, T. Matsumoto, P. B. Kelemen, B. E. Tucholke, and J. F. Casey, Crustal Evolution of the Mid-Atlantic Ridge near the Fifteen-Twenty Fracture Zone in the last 5 Ma, *Geochem. Geophys. Geosyst.*, *4*(3), 1024, doi:10.1029/2002GC000364, 2003.
- Hammer, S., Terrain corrections for gravimeter stations, *Geophysics*, *4*, 184–194, 1939.
- Karson, J. A., Seafloor spreading on the Mid-Atlantic Ridge: implications for the structure of ophiolites and oceanic lithosphere produced in slow-spreading environments, in *Proceedings of the Symposium on Ophiolites and Oceanic Lithosphere - TROODOS 87*, edited by J. Malpas et al., pp. 547–555, Geol. Surv. Dept., Ministry of Agric. and Nat. Resour., Nicosia, Cyprus, 1990.
- Karson, J. A., Geologic investigation of a lineated massif at the Kane transform fault: Implications for oceanic core complexes, *Philos. Trans. R. Soc. London Ser. A*, *357*, 713–736, 1998.
- Kuo, B. Y., and D. W. Forsyth, Gravity anomalies of the ridge-transform system in the South Atlantic between 31 and 34.5°S: Upwelling centers and variations in crustal thickness, *Mar. Geophys. Res.*, *10*, 205–232, 1988.
- Lagabrielle, Y., D. Bideau, M. Cannat, J. A. Karson, and C. Mevel, Ultramafic-mafic plutonic rock suites exposed along the Mid-Atlantic Ridge (10°N–30°N). Symmetrical-

- asymmetrical distribution and implications for seafloor spreading processes, in *Faulting and Magmatism at Mid-Ocean Ridges*, *Geophys. Monogr. Ser.*, vol. 106, edited by W. R. Buck et al., pp. 153–176, AGU, Washington, D. C., 1998.
- Lavier, L. L., W. R. Buck, and A. N. B. Poliakov, Self-consistent rolling-hinge model for the evolution of large- offset low-angle normal faults, *Geology*, *27*, 1127–1130, 1999.
- Lister, G. S., and G. A. Davis, The origin of metamorphic core complexes and detachment faults formed during Tertiary continental extension in the northern Colorado River region, U.S.A., *J. Struct. Geol.*, *11*, 65–94, 1989.
- Luyendyk, B. P., On-bottom gravity profile across the East Pacific Rise crest at 21°N, *Geophysics*, *49*, 2166–2177, 1984.
- MacLeod, C. J., et al., Direct geological evidence for oceanic detachment faulting: The Mid-Atlantic Ridge, 15°45'N, *Geology*, *30*, 879–882, 2002.
- Matsumoto, T., P. B. Kelso, and MODE '98 Leg 1 Scientific Party, Precise geological and geophysical mapping of the 15°20'N Fracture Zone on the MAR - tectonic extension and its consequent exposure of ultramafic and plutonic rocks along the magma-poor ridge axis (MODE '98 Leg 1 Cruise), *InterRidge News*, *7*, 13–17, 1998.
- McAllister, E., and J. Cann, Initiation and evolution of boundary wall faults along the Mid-Atlantic Ridge, 25–29°N, in *Tectonic, Magmatic, Hydrothermal and Biological Segmentation of Mid-Ocean Ridges*, edited by C. J. MacLeod, P. A. Tyler, and C. L. Walker, *Geol. Soc. Spec. Publ.*, *118*, 29–48, 1996.
- Mével, C., et al., Sampling the South West Indian Ridge: First results of the EDUL cruise, *InterRidge News*, *6*, 25–26, 1997a.
- Mével, C., L. M. Parson, K. Tamaki, R. C. Searle, D. Sauter, P. Patriat, P. Blondel, and Fuji Scientific Party, Tectonic and Volcanic Segmentation of the Very Slow Spreading SWIR - New Sidescan Sonar and Swath Bathymetry Data East of 58E, *Eos Trans. AGU*, *78*(46), Fall Meet. Suppl. F683, 1997b.
- Mével, C., et al., Investigating an ultra slow spreading ridge: The first results of the FUJI cruise on the SWIR (R/V Marion Dufresne, 7/10–3/11/97), *InterRidge News*, *7*, 29–32, 1998.
- Parker, R. L., The rapid calculation of potential anomalies, *Geophys. J. R. Astron. Soc.*, *31*, 447–455, 1972.
- Parson, L., E. Gracia, D. Collier, C. German, and D. Needham, Second-order segmentation; the relationship between volcanism and tectonism at the MAR, 38 degrees N–35 degrees 40'N, *Earth Planet. Sci. Lett.*, *178*, 231–251, 2000.
- Patriat, P., et al., The GALLIENI Cruise: A geophysical survey of the South-West Indian Ridge near the Gallieni FZ (37°S, 52°E), *InterRidge News*, *5*, 19–22, 1996.
- Ranero, C. R., and T. J. Reston, Detachment faulting at ocean core complexes, *Geology*, *27*, 983–986, 1999.
- Reston, T. J., W. Weinrebe, I. Grevemeyer, E. R. Flueh, N. C. Mitchell, L. Kirstein, C. Kopp, and H. Kopp, A rifted inside corner massif on the Mid-Atlantic Ridge at 5 degrees S, *Earth Planet. Sci. Lett.*, *200*, 255–269, 2002.
- Searle, R. C., The volcano-tectonic setting of oceanic lithosphere generation, in *Ophiolites and Their Modern Oceanic Analogues*, edited by L. M. Parson, B. J. Murton, and P. Browning, *Geol. Soc. Spec. Publ.*, *60*, 65–80, 1992.
- Searle, R. C., and A. V. Bralee, A geophysical investigation and geological interpretation of a super-slow spreading segment at the South West Indian Ridge (SWIR), *Eos Trans. AGU*, *82*(47), Fall Meet. Suppl., F1097, 2001.
- Searle, R. C., P. A. Cowie, N. C. Mitchell, S. Allerton, C. J. MacLeod, J. Escartin, S. M. Russell, P. A. Slootweg, and T. Tanaka, Fault structure and detailed evolution of a slow spreading ridge segment: The Mid-Atlantic Ridge at 29°N, *Earth Planet. Sci. Lett.*, *154*, 167–183, 1998a.
- Searle, R. C., P. Patriat, G. Pouliquen, C. Mével, and K. Tamaki, TOBI Sdescan Imagery and Magnetics of the Southwest Indian Ridge III: Detailed History and Tectonic Style of Seafloor Spreading and Detachment Faulting, 0–3 Ma, 63°30'E–63°56'E (FUJI Box 3), *Eos Trans. AGU*, *79*(46), Fall Meet. Suppl., F855, 1998b.
- Shemenda, A. I., and A. L. Grocholsky, Physical modelling of slow seafloor spreading, *J. Geophys. Res.*, *99*, 9137–9153, 1994.
- Tucholke, B. E., Relation between Rift-Axis Magmatism, Frequency of Detachment Faulting, and Development of Inside-Corner Highs in Slow-Spreading Crust, *Eos Trans. AGU*, *78*(46), Fall Meet. Suppl., F663, 1997.
- Tucholke, B. E., and J. Lin, A geological model for the structure of ridge segments in slow spreading ocean crust, *J. Geophys. Res.*, *99*, 11,937–11,958, 1994.
- Tucholke, B., J. Lin, and M. Kleinrock, Mullions, megamullions and metamorphic core complexes on the Mid-Atlantic Ridge, *Eos Trans. AGU*, *77*(46), Fall Meet. Suppl., F724, 1996.
- Tucholke, B., J. Lin, M. Kleinrock, M. Tivey, T. Reed, J. Goff, and G. Jaroslow, Segmentation and crustal structure of the western Mid-Atlantic Ridge flank, 25°25'–27°10'N and 0–29 m. y., *J. Geophys. Res.*, *102*, 10,203–210,223, 1997.
- Tucholke, B., J. Lin, and M. Kleinrock, Megamullions and mullion structure defining oceanic metamorphic core complexes on the Mid-Atlantic Ridge, *J. Geophys. Res.*, *103*, 9857–9866, 1998a.
- Tucholke, B. E., K. Fujioka, and T. Ishihara, Shinkai 6500 dives on Dante's Domes, a megamullion in the eastern rift mountains of the Mid-Atlantic Ridge at 26.6 degrees north, *Eos Trans. AGU*, *79*(46), Fall Meet. Suppl., F45, 1998b.
- Tucholke, B. E., K. Fujioka, T. Ishihara, G. Hirth, and M. Kinoshita, Submersible study of an oceanic megamullion in the central North Atlantic, *J. Geophys. Res.*, *106*, 16,145–116,161, 2001.
- Tucholke, B. E., W. R. Buck, L. Lavier, and J. Lin, Investigation of megamullion formation in relation to magma supply, *Geophys. Res. Abstr.*, *5*, Abstract EAE03-A-07925, 2003.
- Varga, R. J., and E. M. Moores, Intermittent magmatic spreading and tectonic extension in the Troodos Ophiolite: Impli-

- cations for exploration for black smoker-type ore deposits, in *Proceedings of the Symposium on Ophiolites and Oceanic Lithosphere - TROODOS 87*, edited by J. Malpas et al., Geol. Surv. Dept., Ministry of Agric. and Nat. Resour., Nicosia, Cyprus, 1990.
- Watts, A., and S. Zhong, *Observations of flexure and the rheology of oceanic lithosphere*, *Geophys. J. Int.*, *142*, 855–875, 2000.
- Wolfe, C. J., G. M. Purdy, D. R. Toomey, and S. C. Solomon, Microearthquake characteristics and crustal velocity structure at 29°N on the Mid-Atlantic Ridge: The architecture of a slow-spreading segment, *J. Geophys. Res.*, *100*, 24,449–424,472, 1995.
- Yin, A., Mechanisms for the formation of domal and basinal detachment faults: A three-dimensional analysis, *J. Geophys. Res.*, *96*, 14,577–514,594, 1991.